Biophysical Journal, Volume 98

Supporting Material

Predicting local SR Ca^{2+} dynamics during Ca^{2+} wave propagation in ventricular myocytes

Hena R. Ramay, M. Saleet Jafri, W. Jonathan Lederer, and Eric A. Sobie

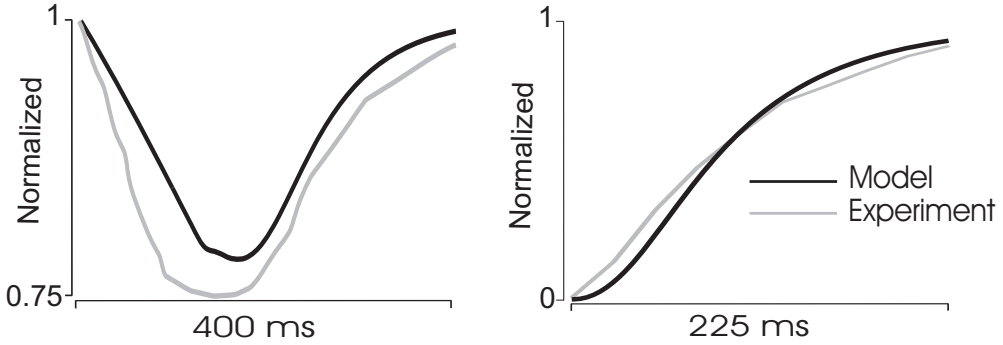

Supplementary Figure S1: Simulation of changes in $[Ca^{2+}]_{SR}$ during a normal Ca^{2+} transient. To validate our parameter choices, we simulated a triggered Ca^{2+} transient during normal excitation-contraction coupling and compared the changes in SR $[Ca^{2+}]$ with the experimental Ca^{2+} "scrap" measurements of Shannon, Guo & Bers (*Circulation Research* 93:440-445, 2003). To simulate a normal Ca^{2+} transient, 10% of the RyR clusters were opened every 15 ms beginning at t=0 until 90% had been triggered at t=120 ms. This release flux duration is comparable to experimentally estimated durations ranging from 80 to 170 ms (Wier et al *Journal of Physiology* 474:463-471, 1994; Song et al *Journal of Physiology* 512:677-691, 1998; Shannon et al *Biophysical Journal* 78: 334–343, 2000) The left plots compare the simulated Ca^{2+} scrap (average of JSR and NSR $[Ca^{2+}]$, weighted by the respective compartment volumes) with the fluorescence measurements from Shannon, Guo, & Bers (their Figure 3B). Each plot is normalized to its maximal value for comparison. The plots at right show only the recovery phases, with each normalized to values between zero and one. Both the simulation results and experimental data show recovery time constants of ~100 ms. These results suggest that our parameter choices are quite reasonable.

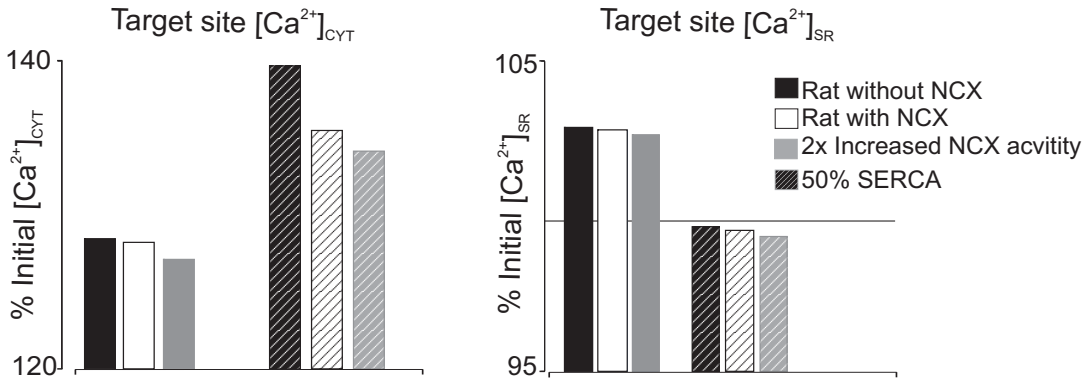

Supplementary Figure S2: Effects of Na^+-Ca^{2+} exchange (NCX). To maintain simplicity, the default model did not include NCX. To assess the extent to which this simplification influenced the model predictions, a separate set of simulations included NCX activity. Simulations performed with the control model (no NCX) were compared with two other sets of results: one that included a "rat-like" NCX that contributed 10% to the decay of a normal Ca^{2+} transient, another with a "rabbit-like" NCX that contributed 25% to the Ca^{2+} transient decay. As expected, including NCX causes a decrease in cytosolic [Ca^{2+}] at the target site (left), and this effect is greater when SERCA is inhibited by 50%. Inclusion of NCX, however, has almost no effect on changes in SR [Ca^{2+}] at the target site (right), with either normal or reduced SERCA activity. This demonstrates that the absence of NCX from the default model does not substantially affect the main conclusions of the study.

NCX activity was modeled using the formulation of Luo & Rudy (*Circulation Research* 74:1071-1096, 1994):

$$I_{NaCa} = k_{NaCa}\frac{(e^{\eta VF/RT}[Na^+]_i^3[Ca^{2+}]_o - e^{(\eta-1)VF/RT}[Na^+]_o^3[Ca^{2+}]_i)}{(K_{m,Na}^3+[Na^+]_o^3)(K_{m,Ca}+[Ca^{2+}]_o)(1+k_{sat}e^{(\eta-1)VF/RT})}$$

where $K_{m,Na}$ and $K_{m,Ca}$ are the Na^+ and Ca^{2+} half-saturation constants, respectively, k_{sat} ensures that the current saturates at extremely negative membrane potentials, and η is the position of the energy barrier that controls the voltage dependence. The scaling factor k_{NaCa}, which controls the maximal NCX current, was 2500 pA/pF for the "rat-like" NCX and 5000 pA/pF for the "rabbit-like" NCX. Values for other parameters are listed below.

Parameter	Definition	Value
A_{cap}	Capacitive membrane area	1.534×10^4 cm^2
C_m	Specific membrane capacitance	1.0 μF/cm^2
F	Faraday constant	96.5 C/mmol
T	Absolute temperature	310 K
R	Ideal gas constant	8.314 J·mol^1·K^1
k_{NaCa}	Scaling factor of Na^+/Ca^{2+} exchange	5000 pA/pF
$K_{m,Na}$	Na^+ half-saturation constant for Na^+/Ca^{2+} exchange	87.5 mM
$K_{m,Ca}$	Ca^{2+} half-saturation constant for Na^+/Ca^{2+} exchange	1.38 mM
k_{sat}	Na^+/Ca^{2+} exchange saturation factor at very negative potentials	0.1
η	Controls voltage dependence of Na^+/Ca^{2+} exchange	0.35
$[Na^+]_o$	External Na^+ concentration	140 mM
$[Na^+]_i$	Intracellular Na^+ concentration	10.2 mM
$[Ca^{2+}]_o$	External Ca^{2+} concentration	6.25 mM

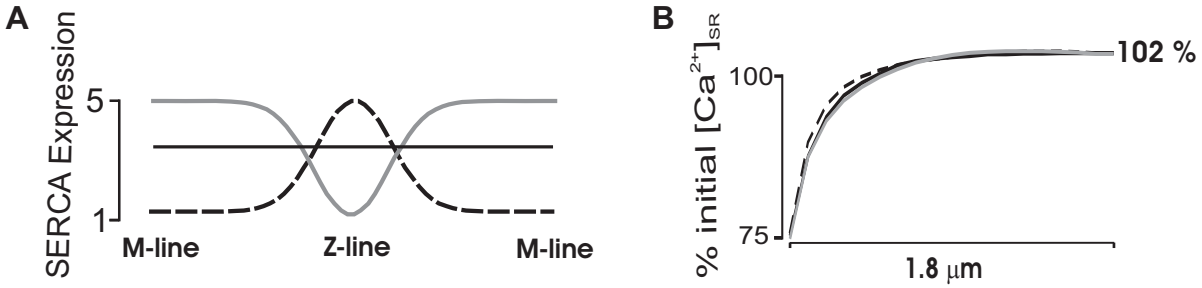

Supplementary Figure S3: Heterogeneous SERCA expression. To test the effects of SERCA distribution (within a sarcomere) on target site $[Ca^{2+}]_{SR}$, we simulated three different distributions: uniform (solid line), increased distribution near the RyR cluster at the Z-line (dashed line) and increased distribution at the center of the sarcomere (gray line). For the solid line, v_{SERCA} = 865 μM/ms everywhere. For the dashed lines, $v_{SERCA} = 865e^{-0.057x}$ μM/ms, where x is the distance from the Z-line in μm. For the gray line, $v_{SERCA} = 1800 - 865e^{-0.057x}$ μM/ms, with x again the distance from the Z-line in μm. The three distributions are shown in **(A)**. The results of the simulations, displayed in **(B)**, show that SERCA distribution has little effect on $[Ca^{2+}]_{SR}$ at the target site. Results for medium $D_{Ca,SR}$ (60 $\mu m^2/s$) are shown.

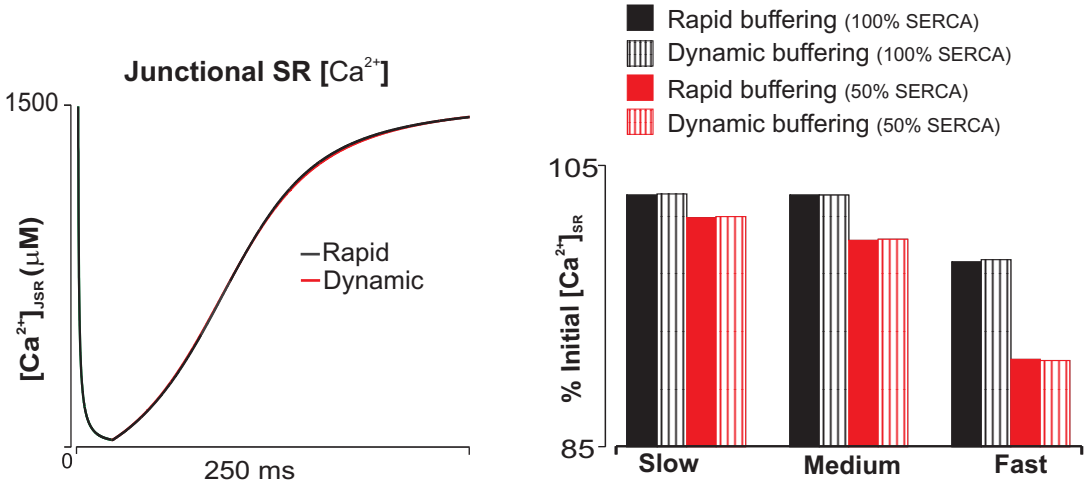

Supplementary Figure S4: Dynamic versus rapid buffering. Two sets of simulations were performed, with conditions otherwise identical: 1) using the rapid buffering approximation to compute Ca^{2+} buffering in the JSR, 2) computing dynamic buffering in the JSR. Results shown are comparisons of the recovery of JSR $[Ca^{2+}]$ after release from a single RyR cluster (left), and of $[Ca^{2+}]_{SR}$ at the target site under different conditions (right). The use of the rapid buffering approximation has no significant effect on the results. In these simulations, medium $D_{Ca,SR}$ (60 $\mu m^2/s$) was assumed.

For the simulations with dynamic buffering, the rate constants were as follows:

Buffer	**k_{on}**	**k_{off}**
Calsequestrin	100 $\mu M^{-1} s^{-1}$	63000 s-1
Juncate	100 $\mu M^{-1} s^{-1}$	21700 s^{-1}